Cysteine as a ligand platform in the biosynthesis of the FeFe hydrogenase H cluster

Daniel L. M. Suess[a], Ingmar Bürstel[b], Liliana De La Paz[b], Jon M. Kuchenreuther[a], Cindy C. Pham[a], Stephen P. Cramer[a], James R. Swartz[b,c], and R. David Britt[a,1]

[a]Department of Chemistry, University of California, Davis, CA 95616; [b]Department of Chemical Engineering, Stanford University, Stanford, CA 94305; and [c]Department of Bioengineering, Stanford University, Stanford, CA 94305

Edited by JoAnne Stubbe, Massachusetts Institute of Technology, Cambridge, MA, and approved August 3, 2015 (received for review May 5, 2015)

Hydrogenases catalyze the redox interconversion of protons and H_2, an important reaction for a number of metabolic processes and for solar fuel production. In FeFe hydrogenases, catalysis occurs at the H cluster, a metallocofactor comprising a $[4Fe–4S]_H$ subcluster coupled to a $[2Fe]_H$ subcluster bound by CO, CN^-, and azadithiolate ligands. The $[2Fe]_H$ subcluster is assembled by the maturases HydE, HydF, and HydG. HydG is a member of the radical *S*-adenosyl-L-methionine family of enzymes that transforms Fe and L-tyrosine into an $[Fe(CO)_2(CN)]$ synthon that is incorporated into the H cluster. Although it is thought that the site of synthon formation in HydG is the "dangler" Fe of a [5Fe] cluster, many mechanistic aspects of this chemistry remain unresolved including the full ligand set of the synthon, how the dangler Fe initially binds to HydG, and how the synthon is released at the end of the reaction. To address these questions, we herein show that L-cysteine (Cys) binds the auxiliary [4Fe–4S] cluster of HydG and further chelates the dangler Fe. We also demonstrate that a $[4Fe–4S]_{aux}[CN]$ species is generated during HydG catalysis, a process that entails the loss of Cys and the $[Fe(CO)_2(CN)]$ fragment; on this basis, we suggest that Cys likely completes the coordination sphere of the synthon. Thus, through spectroscopic analysis of HydG before and after the synthon is formed, we conclude that Cys serves as the ligand platform on which the synthon is built and plays a role in both Fe^{2+} binding and synthon release.

FeFe hydrogenase | metallocofactor biosynthesis | HydG

FeFe hydrogenases catalyze the reversible interconversion of H_2 with protons and electrons, and thereby provide either an electron source or an electron sink for a variety of metabolic processes (1). Hydrogenase reactivity occurs at the H cluster, which consists of a conventional $[4Fe–4S]_H$ subcluster coupled to an organometallic $[2Fe]_H$ subcluster that features a 2-aza-1,3-propanedithiolate ("azadithiolate") ligand and multiple CO and CN^- ligands (Fig. 1*A*) (2, 3). The biosynthesis of the H cluster has garnered much attention (4, 5) given its unusual structure and exceptional H_2 production activity (6). Whereas the $[4Fe–4S]_H$ subcluster is inserted by the housekeeping Fe–S cluster machinery, the $[2Fe]_H$ subcluster is synthesized and inserted by three accessory proteins: the HydE, HydF, and HydG maturases (5, 7–9). Both L-tyrosine (Tyr) and L-cysteine (Cys) have been shown to stimulate in vitro $[2Fe]_H$ subcluster biosynthesis (10, 11) with Tyr serving as the precursor to the CO and CN^- ligands (12–14); the role of Cys in H-cluster maturation is less clear and an emerging area of focus (15).

Significant progress has been made toward elucidating the individual functions of the maturases (5). HydG is a member of the radical *S*-adenosyl-L-methionine (SAM) family of enzymes (16) and performs a complex reaction in which Tyr and Fe are transformed into an $[Fe(CO)_2(CN)]$ synthon that is eventually incorporated into the $[2Fe]_H$ subcluster (17) (Fig. 1*B*). The substrate and product of the radical SAM enzyme HydE are presently unknown, although it is thought that HydE plays a role in building the azadithiolate ligand (5, 15). HydG and HydE are thought to function in concert with the GTP-hydrolyzing enzyme HydF (18, 19) to generate a $[2Fe]_H$ subcluster-like precursor (20–22) that is transferred to the hydrogenase apoprotein (apo-HydA) to yield the mature H cluster. This mechanistic framework continues to undergo substantial refinement as the chemical details of these processes are unraveled.

HydG contains two Fe–S clusters that play separate roles in building the $[Fe(CO)_2(CN)]$ synthon (17, 23–26). Cleavage of Tyr to CO and CN^- is initiated at the N-terminal, SAM-binding $[4Fe–4S]_{RS}$ cluster where one-electron reduction of SAM generates the 5′-deoxyadenosyl radical (5′-dAdo•) (Fig. 1*B*). Subsequent H-atom abstraction from the amino group (27) of Tyr (28) induces Cα–Cβ bond cleavage. The resulting 4-hydroxybenzyl radical (4HOB•) has been observed by EPR spectroscopy (23) indicating that dehydroglycine (DHG) is an intermediate to CO and CN^-; the mechanism of DHG conversion to CO and CN^- is under investigation (29) and beyond the scope of this paper. The auxiliary, C-terminal cluster adopts an $S = 5/2$ spin state and is proposed to be the site of $[Fe(CO)_2(CN)]$ synthon formation (17, 26). The X-ray crystal structure of chemically reconstituted *Carboxydothermus hydrogenoformans* HydG features a $[4Fe–4S]_{RS}$ cluster, however no auxiliary cluster was observed (25). On the other hand, an X-ray crystal structure of chemically reconstituted *Thermoanaerobacter italicus* (*Ti*) HydG shows the auxiliary cluster in a structurally unprecedented $[5Fe–5S]_{aux}$ form, consisting of a conventional [4Fe–4S] cluster linked via a bridging sulfide to a partially occupied dangler Fe (26). In this structure, the dangler Fe is further ligated by a histidine residue and a nonproteinaceous, unidentified amino acid via its carboxylate and amino groups; this unidentified amino acid was suggested to be mechanistically irrelevant (26). Support for a $[5Fe]_{aux}$ cluster was also obtained from EPR spectroscopic studies of *Shewanella oneidensis* (*So*) HydG (26). Taken together, these results point to the dangler Fe as the site for synthon formation.

Significance

Hydrogen production is central to a solar fuel paradigm, and a variety of metabolic processes use H_2 as an electron donor or protons as an electron acceptor. Hydrogenases mediate the biological redox interconversion of protons and H_2, with FeFe hydrogenases among the most active. This reactivity occurs at the "H cluster," which features an organometallic subcluster that is synthesized and inserted in a complex series of steps. The accessory protein HydG generates an $[Fe(CO)_2(CN)]$ intermediate en route to the H cluster, and the mechanism of this process is under intensive investigation. We now report that free L-cysteine serves as the ligand platform on which the $[Fe(CO)_2(CN)]$ synthon is built and plays a role in both Fe^{2+} binding and synthon release.

Author contributions: D.L.M.S., I.B., L.D.L.P., S.P.C., J.R.S., and R.D.B. designed research; D.L.M.S., I.B., L.D.L.P., J.M.K., and C.C.P. performed research; D.L.M.S., I.B., L.D.L.P., S.P.C., J.R.S., and R.D.B. analyzed data; and D.L.M.S., I.B., L.D.L.P., J.M.K., C.C.P., S.P.C., J.R.S., and R.D.B. wrote the paper.

The authors declare no conflict of interest.

This article is a PNAS Direct Submission.

[1]To whom correspondence should be addressed. Email: rdbritt@ucdavis.edu.

This article contains supporting information online at www.pnas.org/lookup/suppl/doi:10.1073/pnas.1508440112/-/DCSupplemental.

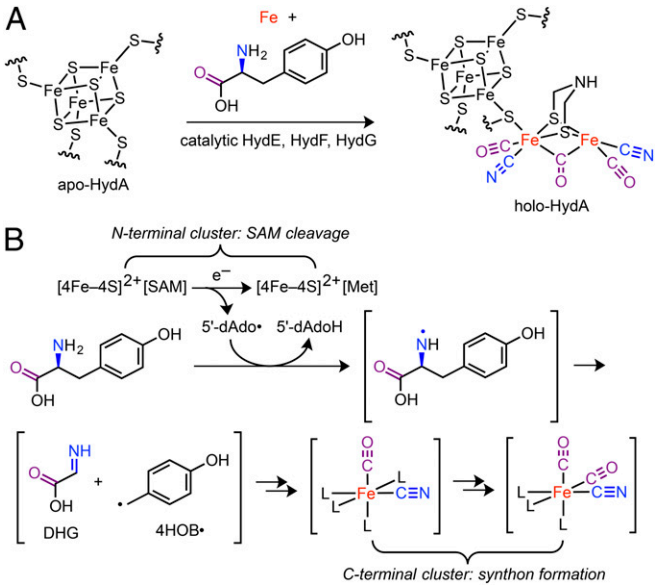

Fig. 1. Overview of FeFe hydrogenase (HydA) H-cluster bioassembly. (*A*) Maturation of apo-HydA. (*B*) The reaction promoted by HydG. Met = L-methionine; 5′dAdoH = 5′-deoxyadenosine; other abbreviations as noted in the text.

In this work, we report spectroscopic studies of HydG before $[Fe(CO)_2(CN)]$ synthon formation and after synthon release, including evidence for exogenous Cys binding to the dangler Fe and formation of a $[4Fe–4S]_{aux}[CN]$ species during turnover. Based on these results, we propose a mechanism in which Cys serves as the ligand platform on which the synthon is built and discuss its role in Fe binding and release.

Results

Wild-type (WT) *So*HydG ("HydG") was expressed in *Escherichia coli* BL21(DE3) Δ*iscR::kan* and purified using StrepTactin affinity chromatography as previously described (12). Typical X-band EPR spectra of HydG samples reduced by dithionite (DTH) show two distinct signals: an $S = 1/2$ signal near $g = 2$ that corresponds to the $[4Fe–4S]^+_{RS}$ cluster and an unusual $S = 5/2$ signal with resonances at $g_{eff} = 9.5$, 4.7, 4.1, and 3.8 that corresponds to the C-terminal, auxiliary cluster (Fig. 2 and *SI Appendix*, Fig. S1) (23, 26). In light of the crystallographically observed *Ti*HydG auxiliary cluster structure, the $S = 5/2$ spin system observed by EPR spectroscopy may be understood as resulting from

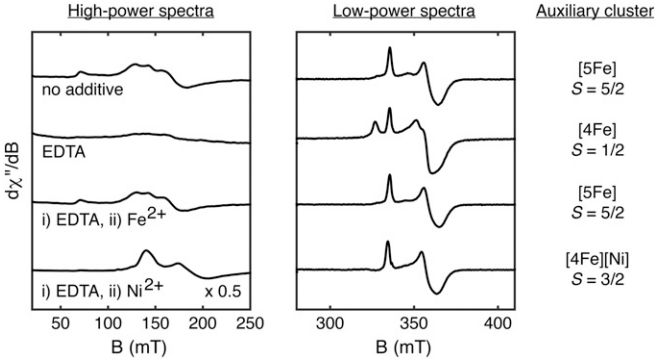

Fig. 2. Studies of dangler metal ion removal and incorporation. X-band EPR spectra of DTH-reduced HydG recorded at 10 K with 5-mW (*Left*) or 126-μW (*Right*) power.

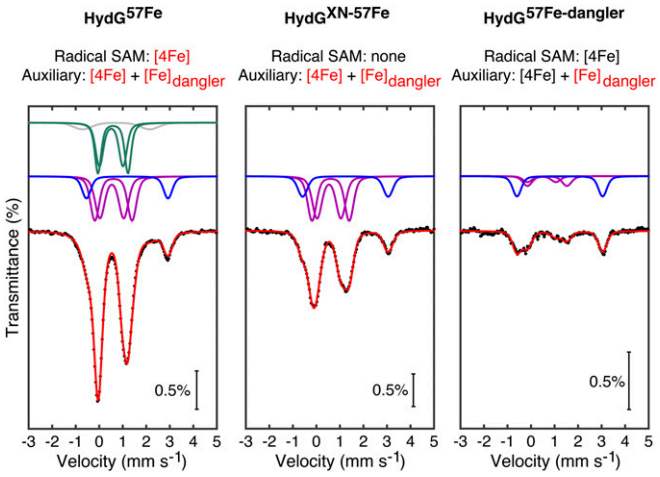

Fig. 3. Mössbauer spectra (zero field, 80 K) of HydG with the total fit (red) and components corresponding to the dangler Fe^{2+} (blue), the $[4Fe–4S]^+_{aux}$ (purple) and $[4Fe–4S]^+_{RS}$ (green) mixed valence pairs, and adventitiously bound Fe (gray) (see Table 1 and *SI Appendix* for fitting details). Red text indicates ^{57}Fe labeling.

exchange coupling between an $S = 2$ dangler Fe^{2+} and an $S = 1/2$ $[4Fe–4S]^+_{aux}$ subcluster (*SI Appendix*, Fig. S2) (26).

The dangler Fe in HydG may be selectively and reversibly removed by treatment with the metal chelating agent EDTA, resulting in conversion of the $S = 5/2$ $[5Fe]_{aux}$ cluster to an $S = 1/2$ $[4Fe]_{aux}$ cluster (Fig. 2). Subsequent addition of excess Fe^{2+} cleanly regenerates the $S = 5/2$ EPR signal of the $[5Fe]_{aux}$ cluster. This procedure allows for other metals to be installed into the dangler position to give nonnative, heteronuclear clusters. For example, addition of Ni^{2+} converts the $S = 1/2$ signal to a new $S = 3/2$ signal, as indicated by resonances at $g_{eff} = 4.8$ and 3.6. This spin system is consistent with a dangler $S = 1$ Ni^{2+} center that is exchange-coupled to the $S = 1/2$ $[4Fe–4S]^+_{aux}$ subcluster (*SI Appendix*, Fig. S2) and is reminiscent of that observed for the $S = 3/2$ form of the NiFe CO dehydrogenase α-subunit (30).

The reversible [5Fe]↔[4Fe] conversion of the HydG auxiliary cluster was also studied by Mössbauer spectroscopy. $HydG^{XN}$—a mutant wherein the three Cys residues that bind the $[4Fe–4S]_{RS}$ cluster have been mutated to Ser residues (26)—was expressed in cells grown on ^{57}Fe-containing medium ("$HydG^{XN\text{-}57Fe}$") to give a sample that contains only the ^{57}Fe-labeled auxiliary cluster. The zero-field Mössbauer spectrum of this sample consists of three doublets (Fig. 3, *Center*): two that correspond to the $[Fe^{2+}Fe^{2+}]$ and $[Fe^{2.5+}Fe^{2.5+}]$ pairs of the $[4Fe–4S]^+_{aux}$ subcluster (31) and one that is characteristic of a six-coordinate, $S = 2$ Fe^{2+} site which may therefore be ascribed to the dangler Fe; least-squares fitting of this spectrum yielded the expected 2:2:1 ratio of integrated areas, respectively (Table 1). The Mössbauer spectrum of globally ^{57}Fe-labeled WT HydG ("$HydG^{57Fe}$") is similar in its features with additional intensity corresponding to the $[4Fe–4S]^+_{RS}$ cluster (Fig. 3, *Left* and Table 1). In a separate sample, the dangler Fe of natural-abundance WT HydG was removed by treatment with EDTA and subsequently reinstalled using $^{57}Fe^{2+}$ ("$HydG^{57Fe\text{-}dangler}$"). The resulting Mössbauer spectrum (Fig. 3, *Right*) features the dangler Fe doublet as the predominant signal (~55%); the remaining $[4Fe–4S]^+$ cluster signal intensity (~45%) indicates some ^{57}Fe exchange with the [4Fe–4S] clusters during sample preparation with a ~10:1 average selectivity for labeling the dangler Fe over any other single Fe site (Table 1). This study constitutes one of a few examples of site-selective ^{57}Fe labeling of Fe–S clusters (32, 33).

Although most samples of as-isolated HydG and $HydG^{XN}$ display an intense $S = 5/2$ EPR signal corresponding to the

Table 1. Mössbauer fitting parameters corresponding to Fig. 3

Site	δ, mm s^{-1}	ΔE_Q, mm s^{-1}	Area, %	Relative area
HydG^{57Fe}				
$[4Fe–4S]^+_{aux}$	0.61*,†	1.58*	21.9	2*,†
	0.53*	1.02*	21.9	2*,†
Dangler Fe^{2+}	1.19	3.47	11.0	1*
$[4Fe–4S]^+_{RS}$	0.58	1.27	19.4	1.8
	0.51	1.00	19.4	1.8
Other Fe	0.72	2.85	6.4	0.6
HydG^{XN57Fe}				
$[4Fe–4S]^+_{aux}$	0.61	1.58	40.1	2.0†
	0.53	1.02	40.1	2.0†
Dangler Fe^{2+}	1.23	3.64	19.9	1
HydG$^{57Fe\text{-}dangler}$				
$[4Fe–4S]^+$	0.68‡	1.68‡	28.1‡	0.8
	0.45‡	1.20‡	16.9‡	
Dangler Fe^{2+}	1.22	3.64	55.0	1

*Parameters were determined using the HydG^{XN57Fe} sample and fixed during spectral fitting.

†The intensities of the $[Fe^{2+}Fe^{2+}]$ and $[Fe^{2.5+}Fe^{2.5+}]$ doublets for each $[4Fe–4S]^+$ cluster were fixed to be equal.

‡Because of the low intensity of the $[4Fe–4S]^+$ cluster doublets in this sample, these fitting parameters are likely not accurate. Rather, they were used to obtain a close fit to the data to estimate the total intensity of the $[4Fe–4S]^+$ cluster doublets relative to that of the dangler Fe^{2+} doublet.

$[5Fe]_{aux}$ form (Fig. 2 and *SI Appendix*, Fig. S1), some samples exhibit additional $S = 1/2$ EPR signals of variable intensity, suggesting that the auxiliary cluster is present in one or more $[4Fe]_{aux}$ forms. An extreme case is shown for a specific HydG^{XN} sample in which little of the distinctive $S = 5/2$ EPR signal from the $[5Fe]_{aux}$ form is present (Fig. 4*A*). We do not currently understand why some preparations result in partially degraded auxiliary clusters. Nevertheless, this sample of dangler-deficient HydG^{XN} afforded the opportunity to investigate the reconstitution to the $[5Fe]_{aux}$ form. Based on the $[5Fe–5S]_{aux}$ cluster formulated for *Ti*HydG (26), our initial experiments focused on the effects of added Fe^{2+} and S^{2-}. Incubation with Fe^{2+} results in conversion of some of the $S = 1/2$ $[4Fe–4S]^+_{aux}$ signal intensity into higher-spin forms (Fig. 4*A*); however, subsequent addition of S^{2-} gave little further change to the cluster composition (Fig. 4*A*), suggesting that S^{2-} is not necessary for $[5Fe]_{aux}$ cluster formation and that another component is needed for complete reconstitution.

Given the observation of the unidentified amino acid in the *Ti*HydG structure (26) as well as the finding that Cys stimulates hydrogenase maturation (10, 11), we hypothesized that the auxiliary cluster could be composed of a $[4Fe–4S]_{aux}$ cluster linked to the dangler Fe via a nonproteinaceous Cys thiolate (rather than via a bridging S^{2-} ligand). Addition of Cys to dangler-deficient HydG^{XN} gives an appreciable increase in the $S = 5/2$ $[5Fe]_{aux}$ signal at the expense of some $S = 1/2$ $[4Fe–4S]^+_{aux}$ signal intensity (Fig. 4*A*), and adding both Cys and Fe^{2+} gives complete conversion to the $[5Fe]_{aux}$ signal (Fig. 4*A*). These results indicate that the auxiliary cluster in the HydG^{XN} samples used for this reconstitution study initially adopts structures that are deficient in Fe, Cys, or both Fe and Cys. Finally, treatment of dangler-deficient HydG^{XN} with Cys and EDTA results in nearly quantitative formation of an $S = 1/2$ signal (g = [2.06, 1.90, 1.87]; Fig. 4*A* and *SI Appendix*, Fig. S3) that we assign to a $[4Fe–4S]_{aux}$[Cys] cluster (*vide infra*). This signal is also observed upon EDTA addition to nonreconstituted samples of WT HydG (Fig. 2), suggesting that Cys binds to the auxiliary cluster in the as-isolated protein.

Based on these findings, we conclude that the $[5Fe]_{aux}$ cluster has a $[4Fe–4S]_{aux}[(\kappa^3\text{-Cys})Fe]$ structure with the Cys ligand binding the dangler Fe in a tridentate mode via its carboxylate, amino, and thiolate donors and that EDTA treatment gives a $[4Fe–4S]_{aux}$[Cys] cluster (Fig. 4*B*). This proposal is based in part on the coordination geometry of the unidentified amino acid about the dangler Fe in the *Ti*HydG crystal structure (26). Although we argue in favor of a native $[4Fe–4S]_{aux}[(\kappa^3\text{-Cys})Fe]$ cluster structure, the crystallographically observed *Ti*HydG auxiliary cluster may have a different [5Fe] composition (e.g. a $[5Fe–5S]_{aux}$ cluster as originally reported [26]).

In addition, we have found that Fe^{2+} and Cys are the only additives that convert $S = 1/2$ $[4Fe–4S]^+_{aux}$ signals to the distinctive $S = 5/2$ $[5Fe]_{aux}$ signal that is observed in most samples of nonreconstituted HydG and HydG^{XN}; reconstitution trials in which L-Cys is replaced by D-cysteine, L-homocysteine, L-alanine + S^{2-}, or L-serine do not restore the $S = 5/2[5Fe]_{aux}$ signal (Fig. 4*A* and *SI Appendix*, Fig. S4), suggesting that the auxiliary cluster binding site is specifically tailored for L-Cys. The observed binding specificity may be rationalized by the presence of two conserved residues (S342 and Q343, *SI Appendix*, Fig. S5) that serve as putative H-bond donors to the carboxylate group of the unidentified amino acid in the *Ti*HydG crystal structure (26).

To further probe the nature of Cys binding to the auxiliary cluster, we characterized the $[4Fe–4S]_{aux}$[Cys] form in the presence of isotopically labeled Cys using electron-nuclear double resonance (ENDOR) spectroscopy. For this purpose, dangler- and Cys-deficient samples of HydG (that would otherwise require reconstitution with Fe^{2+} and Cys) were incubated with excess ^{15}N-$^{13}C_3$-Cys or 3-^{13}C-Cys and treated with EDTA to remove any dangler Fe (*SI Appendix*, Fig. S6). The orientation-selected Mims

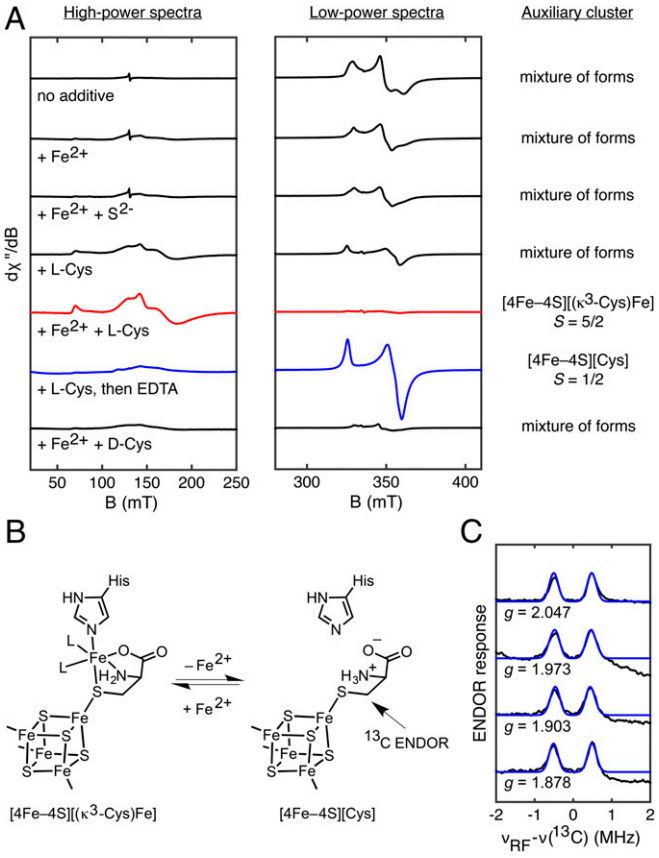

Fig. 4. Cys binding to the auxiliary cluster. (*A*) X-band EPR spectroscopic studies of auxiliary cluster reconstitution in dangler- and Cys-deficient, DTH-reduced HydG^{XN} recorded at 10 K with 5-mW (*Left*) or 126-μW (*Right*) power. (*B*) Scheme showing reversible dangler Fe^{2+} binding. (*C*) Q-band Mims ENDOR spectra of HydG treated with DTH, SAM, and EDTA in the presence of 3-^{13}C-Cys (black) with simulations (blue) using $A(^{13}C)$ = [0.83, 0.83, 1.09] MHz and Euler angles of [0°, 40°, 0°].

ENDOR spectra of the sample prepared with 3-^{13}C-Cys (Fig. 4*C*) display a relatively isotropic hyperfine coupling tensor of $A(^{13}C)$ = [0.83, 0.83, 1.09] MHz with associated Euler angles of [0°, 40°, 0°]. Comparison with the Mims ENDOR spectrum of the sample prepared with ^{15}N-$^{13}C_3$-Cys reveals that the 3-^{13}C nucleus is the most strongly coupled (*SI Appendix*, Fig. S7). These findings are consistent with Cys-thiolate coordination as depicted in Fig. 4*B*.

We studied the fate of Cys during [Fe(CO)$_2$(CN)] synthon formation through EPR spectroscopic examination of HydG-catalyzed reaction mixtures (with added DTH, Tyr, and SAM) that were incubated for 20 min before freezing—conditions that lead to [Fe(CO)$_2$(CN)] synthon formation as previously shown by stopped-flow (SF)-FTIR spectroscopy (17). For these studies, HydG samples were used in which the auxiliary cluster was in its typical [4Fe–4S]$_{aux}$[(κ^3-Cys)Fe] form. EPR spectra of these 20-min reaction mixtures display several signals (Fig. 5*A* and *SI Appendix*, Fig. S8), one of which is characterized by g = [2.09, 1.94, 1.93]. This signal is also observed in samples of HydG treated with KCN in the absence of Tyr and SAM (under nonreaction conditions) and was previously identified as a [4Fe–4S]$_{aux}$[CN] species using hyperfine sublevel correlation (HYSCORE) spectroscopy (26). To test if this [4Fe–4S]$_{aux}$[CN] species is formed during the HydG reaction, we recorded X-band HYSCORE spectra of 20-min reaction samples prepared with 2-^{13}C-Tyr or ^{15}N-Tyr to selectively ^{13}C- or ^{15}N-label any CN$^-$-containing intermediates. Both sets of HYSCORE spectra match those of the K^{13}CN- or KC^{15}N-treated HydG samples, respectively (Fig. 5 *C* and *D*), proving that the [4Fe–4S]$_{aux}$[CN] species builds up during the reaction (Fig. 5*B*).

Importantly, the [4Fe–4S]$_{aux}$[CN] species can only form after the dangler Fe—along with its Cys, CO, and CN$^-$ ligands—has been released from the [4Fe–4S]$_{aux}$ cluster. Thus, the [Fe(CO)$_2$(CN)] synthon likely also contains Cys and may therefore be formulated as the small-molecule complex [(κ^3-Cys)Fe(CO)$_2$(CN)]$^-$ (Fig. 6*A* and *SI Appendix*, Table S1 and Fig. S9). A small-molecule synthon such as [(κ^3-Cys)Fe(CO)$_2$(CN)]$^-$ may not be stable outside of the protein environment and as such would be handed off directly to its downstream acceptor. Consistent with this proposal, we have thus far been unable to observe any organometallic products in solution by electrospray ionization mass spectrometry.

Finally, we investigated whether Cys can substitute for CN$^-$ at the [4Fe–4S]$_{aux}$ cluster to regenerate the [4Fe–4S]$_{aux}$[Cys] form. Indeed, addition of Cys to the [4Fe–4S]$_{aux}$[CN] form (initially generated by addition of KCN) results in complete conversion of the S = 1/2 [4Fe–4S]$_{aux}$[CN] signal to the S = 1/2 [4Fe–4S]$_{aux}$[Cys] signal (Fig. 5 *A* and *B*). The facile displacement of CN$^-$ by Cys may be rationalized by both the strong binding of Cys (*vide supra*) and the relatively weak binding of CN$^-$; the latter has been observed in both biological (34) and synthetic (35) [4Fe–4S] clusters. This experiment demonstrates that regeneration of the [4Fe–4S]$_{aux}$[Cys] species is a plausible step in the HydG catalytic cycle (*vide infra*).

Discussion

With these studies of dangler Fe removal and insertion, Cys binding at the auxiliary cluster, and the [4Fe–4S]$_{aux}$[CN] species observed during HydG catalysis, there is now spectroscopic support for each of the species shown in Fig. 6*A* as well as evidence for their interconversion. At the start of the reaction, the dangler Fe is loaded into the [4Fe–4S]$_{aux}$[Cys] cluster to give the [4Fe–4S]$_{aux}$[(κ^3-Cys)Fe] form; alternatively, a (Cys)Fe complex could be loaded into HydG with Cys serving as a chaperone for Fe insertion. After SAM-mediated cleavage of Tyr, CO and CN$^-$ are generated, resulting in an [Fe(CO)(CN)] complex that was

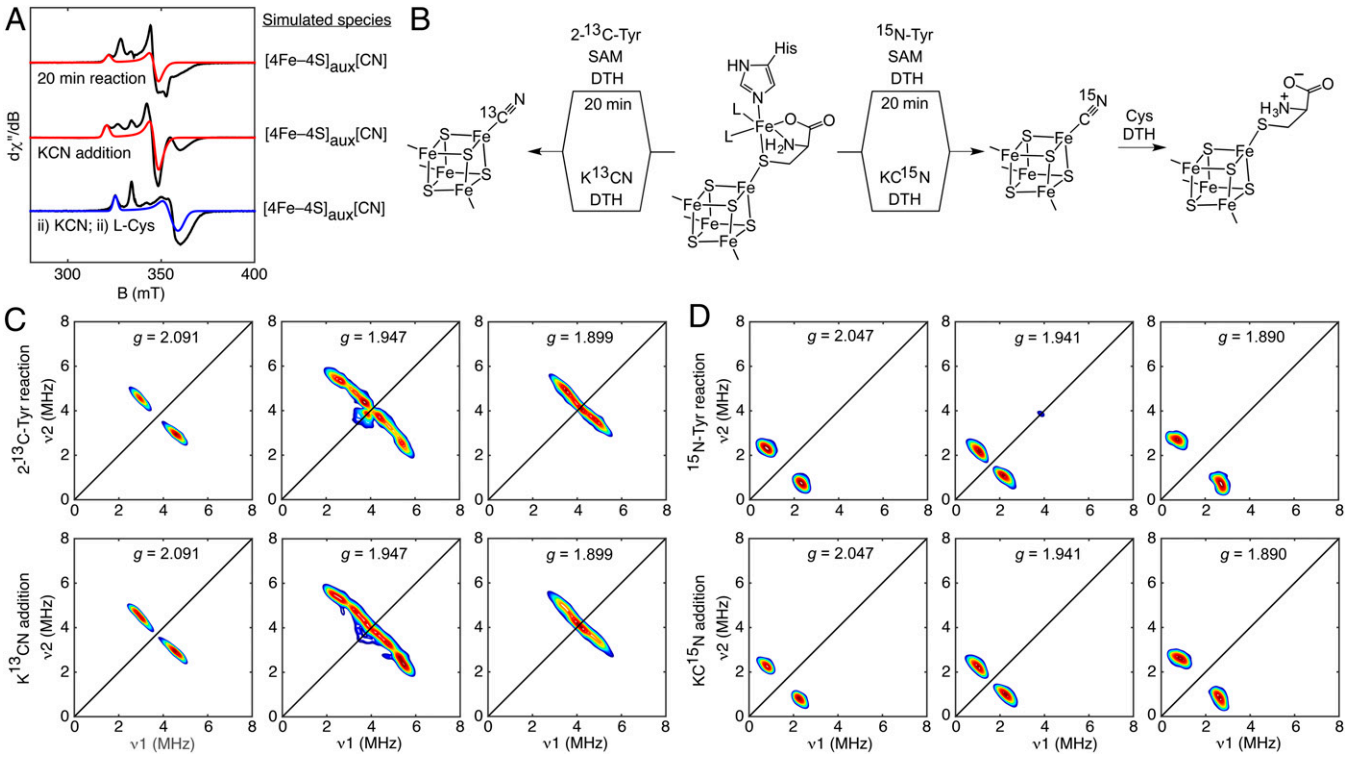

Fig. 5. Formation and ligand substitution reactivity of the [4Fe–4S]$^+_{aux}$[CN] species. (*A*) X-band EPR spectra of HydG recorded at 20 K (top and middle traces) or 10 K (bottom trace) with 126-μW power (black: data; red: simulation of the [4Fe–4S]$_{aux}$[CN] signals; blue: simulation of the [4Fe–4S]$_{aux}$[Cys] signal). (*B*) Scheme showing formation of the [4Fe–4S]$_{aux}$[CN] form and further transformation to the [4Fe–4S]$_{aux}$[Cys] cluster form. (*C*) Orientation-selected X-band HYSCORE spectra of DTH-reduced HydG after a 20-min reaction using SAM and 2-^{13}C-Tyr (*Top*) or after addition of K^{13}CN (*Bottom*; reproduced from ref. 26). (*D*) Orientation-selected X-band HYSCORE spectra of DTH-reduced HydG after a 20-min reaction using SAM and ^{15}N-Tyr (*Top*) or after addition of KC^{15}N (*Bottom*).

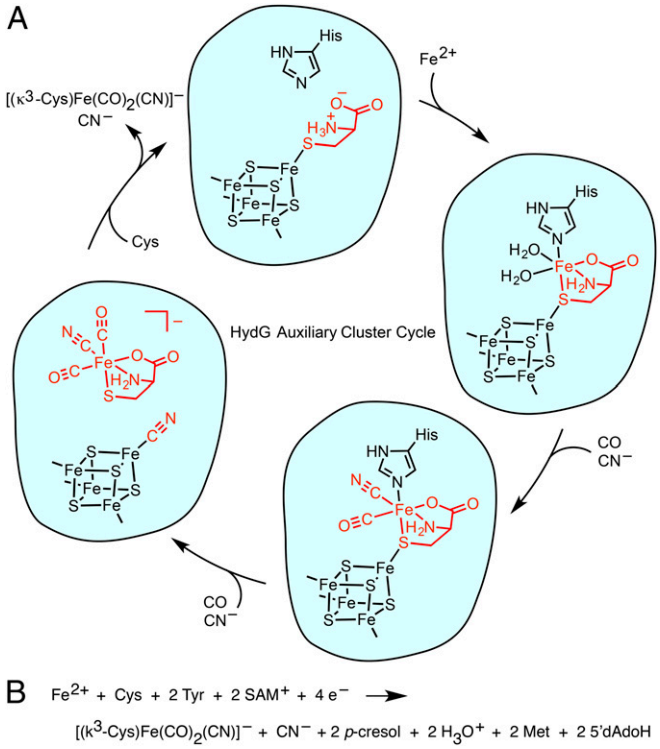

Fig. 6. (*A*) Proposed mechanism for synthon formation and release from the auxiliary cluster. Only one stereoisomer of each organometallic species is shown. (*B*) Proposed net HydG reaction.

previously observed by SF-FTIR (17). A second Tyr cleavage event results in formation of the $[4Fe–4S]_{aux}[CN]$ species and the organometallic synthon which we formulate as the $S = 0$ complex $[(\kappa^3\text{-Cys})Fe(CO)_2(CN)]^-$. The CN^- ligand derived from the second Tyr cleavage event may be directly involved in product release by functioning as a nucleophile that displaces the synthon from the $[4Fe–4S]_{aux}$ cluster. Subsequent displacement of CN^- by Cys [or a (Cys)Fe complex] at the $[4Fe–4S]_{aux}$ cluster could prime the enzyme for another turnover. The mechanism outlined in Fig. 6*A* therefore implies the net HydG reaction shown in Fig. 6*B*.

This mechanistic proposal accounts for the discrepancy between the 3:2 ratio of $CO:CN^-$ ligands in the $[2Fe]_H$ subcluster (Fig. 1) and the assumption that each HydG-mediated Tyr cleavage event should produce equal quantities of CO and CN^-. If the biosynthesis of one $[2Fe]_H$ subcluster entails formation of two $[(\kappa^3\text{-Cys})Fe(CO)_2(CN)]^-$ synthons, then four HydG-mediated Tyr cleavage events must occur, requiring the loss of one CO and two CN^- ligands during maturation. The formation of two $[(\kappa^3\text{-Cys})Fe(CO)_2(CN)]^-$ synthons and two $[4Fe–4S]_{aux}[CN]$ equivalents accounts for the requisite loss of two CN^- ligands in the manner described above. A CO ligand may then be lost at a later stage in maturation to give the 3:2 ratio of $CO:CN^-$ that is observed for all redox states except for H_{ox}–CO (4). One illustration of such a process is the loss of CO upon incorporation of the synthetic $[Fe_2(CO)_4(CN)_2(azadithiolate)]^{2-}$ precursor into apo-HydA (36).

The evidence presented for Cys coordination to the HydG auxiliary cluster may clarify the discrepancies about the Fe–S cluster composition of HydG (*SI Appendix*, Table S2). Although *So*HydG has been shown to harbor an $S = 5/2$ cluster (which we identify here as the $[4Fe–4S]_{aux}[(\kappa^3\text{-Cys})Fe]$ form) (23, 26), EPR spectroscopic investigations of *Thermatoga maritima* (*Tm*) and *Clostridium acetobutylicum* (*Ca*) HydG identified multiple $S = 1/2$ EPR signals and on this basis suggested a conventional $[4Fe–4S]_{aux}$ cluster structure (14, 24, 37). These *Tm*HydG and *Ca*HydG samples were purified using metal-affinity chromatography with subsequent chemical reconstitution using Fe and S^{2-}; however, Cys was not included during reconstitution, which may explain the absence of the $[4Fe–4S]_{aux}[(\kappa^3\text{-Cys})Fe]$ cluster in these samples. Conversely, the previously reported *So*HydG preparation employs a *Strep*-II tag (11) which allows for gentler chromatographic purification, usually obviating the need for Fe–S cluster reconstitution. Thus, *So*HydG isolated in this manner is typically preloaded with both Cys and the dangler Fe and is likely reflective of the Fe–S cluster composition during both in vivo and in vitro (11) H-cluster maturation.

The finding that Cys binds to the dangler Fe provides some chemical insights into its stimulatory effects on FeFe hydrogenase maturation (10, 11). At the start of the HydG reaction, Cys promotes Fe^{2+} binding either as a chelator that is already bound to the auxiliary cluster (Fig. 6*A*), or as a chaperone in which a $(Cys)Fe^{2+}$ complex is inserted into HydG. Cys then serves as the supporting ligand platform on which the $[Fe(CO)_2(CN)]$ synthon is built. Its ensuing fate is unclear. One possibility is that, upon transfer of HydG's organometallic product to its downstream acceptor (likely HydF), Cys simply dechelates, and thereby functions as a carrier for the synthon. Another possibility is that Cys functions as a substrate in a series of complex reactions with HydE and/or HydF, being transformed into part of the azadithiolate ligand in the $[2Fe]_H$ subcluster (10, 15). In either scenario, the hard, weak-field Cys amino and carboxylate donors are well matched for high-spin Fe and poorly matched for low-spin Fe; in this regard, Cys is well suited for performing the delicate balancing act of binding high-spin Fe^{2+} with high affinity at the start of the HydG reaction and releasing the low-spin $[Fe(CO)_2(CN)]$ synthon.

Materials and Methods

Materials. Nonisotopically enriched chemicals were purchased from common commercial vendors. Isotopically enriched chemicals (3-^{13}C-L-cysteine, ^{15}N-$^{13}C_3$-L-cysteine, ^{15}N- L-tyrosine, 2-^{13}C- L-tyrosine, K^{13}CN, and KC^{15}N) were purchased from Cambridge Isotope Laboratories. All additives except for tyrosine were dissolved in 50 mM Hepes buffer (pH = 7.5) with 50 mM KCl and adjusted to pH = 7.5 before use. Tyrosine solutions were prepared as previously described (23). ^{57}Fe solutions were prepared as previously described (38).

Protein Expression and Purification. *S. oneidensis* WT HydG ("HydG"), HydG^{XN}, and HydG^{XC} [also called "HydG^{5xx5}" (23)] were expressed in *E. coli* BL21(DE3) Δ*iscR::kan* cells, purified using a StrepTactin-Sepharose column as previously described (11, 12, 26), and frozen before the preparation of spectroscopic samples. ^{57}Fe-labeled samples were generated as previously described (17).

Spectroscopic Sample Preparation. EPR and Mössbauer samples were prepared in an anaerobic glove box under a N_2 atmosphere (<1 ppm O_2) and frozen using liquid nitrogen before spectroscopic analysis. All samples made for the reconstitution studies in Fig. 4*A* and *SI Appendix*, Fig. S4 were prepared identically. Unless otherwise indicated, the final substrate concentrations for these samples and all other samples were as follows: freshly thawed HydG, ~200–1,000 μM; DTH, 10 mM; all other additives, 3 mM. Other than HydG, each component was added as a solution of 10-fold higher concentration than its final concentration. For example, addition of DTH (6 μL at 100 mM), SAM (6 μL at 30 mM), Fe^{2+} (6 μL at 30 mM), and Cys (6 μL at 30 mM) to HydG (36 μL at 750 μM) gives a Cys- and Fe-reconstituted sample of HydG. For the reconstitution studies in Fig. 4*A* and *SI Appendix*, Fig. S4, reagents were added in the following order: DTH, SAM, Fe^{2+}, then other additives with S^{2-} being last. Twenty-minute HydG reaction samples were prepared using DTH (3 mM), SAM, and either ^{15}N-Tyr or 2-^{13}C-Tyr as previously described (23). HydG^{57Fe} and HydG$^{57Fe\text{-}dangler}$ Mössbauer samples were prepared with DTH, SAM, and Cys. HydG$^{XN\text{-}57Fe}$ Mössbauer samples were prepared with DTH and Cys.

Protocol for Dangler Fe Removal and Subsequent Reinstallation. DTH, SAM, Cys, and EDTA solutions were added to a freshly thawed solution of HydG (in that order). The resulting solution was mixed gently and allowed to stand at room temperature for 20 min. The solution was then diluted 10-fold with

buffer containing DTH, SAM, and Cys and subsequently concentrated 10-fold using an Amicon centrifugal filter (30-kDa cutoff). When applicable, the samples were further treated with Fe^{2+}, $^{57}Fe^{2+}$, or Ni^{2+}. EPR samples were then frozen for spectroscopic analysis. The procedure for preparing $HydG^{XN}$ samples is identical to that for WT HydG except SAM is omitted. The WT $HydG^{57Fe\text{-}dangler}$ Mössbauer sample was prepared with the following additional series of steps before freezing to ensure rigorous removal of excess $^{57}Fe^{2+}$: after addition of $^{57}Fe^{2+}$, the sample was diluted 10-fold with buffer containing DTH, SAM, and Cys, and subsequently concentrated 10-fold. This series of steps was performed a total of three times.

KCN Treatment Followed by CN^- Displacement by Cys. DTH, SAM, and 15 mM $K^{13}CN$ (or $KC^{15}N$) were added to a freshly thawed solution of HydG (in that order). The solution was mixed gently and allowed to stand at room temperature for 20 min. The solution was then diluted 10-fold with buffer containing DTH, SAM, and Cys (or no Cys for the control experiment) and subsequently concentrated 10-fold using an Amicon centrifugal filter (30 kDa cutoff) to give the $[4Fe\text{–}4S]_{aux}$[Cys] form (or the $[4Fe\text{–}4S]_{aux}$[CN] form for the control experiment). This procedure was adapted from a previously reported protocol (26).

EPR Spectroscopic Methods. X-band continuous-wave EPR spectra were recorded at 9.4 GHz using 5.0 G modulation amplitude. HYSCORE spectra were recorded at 9.7–9.8 GHz and 10 K using the pulse sequence $\pi/2$-τ-$\pi/2$-t1-π-t2-$\pi/2$-τ-echo, wherein both the excitation and the inversion pulse lengths are identical (16 ns). Values of τ were chosen to suppress ^{1}H nuclear coherences (τ = 128–140 ns). Mims ENDOR spectra were acquired in stochastic mode at 34.0 GHz and 7 K. The $\pi/2$-τ-$\pi/2$-π_{RF}-$\pi/2$-τ-echo pulse sequence was used with an excitation pulse length of 16 ns, an rf pulse length of 20 μs, and τ value of 220 ns. Spectral simulations were performed with MATLAB using the EasySpin 4.5.5 toolbox (39). See *SI Appendix*.

Mössbauer Spectroscopic Methods. Mössbauer spectra were recorded at zero field on a See Co. MS4 spectrometer equipped with a Janis SVT-400 cryostat. Spectra were calibrated using an Fe foil standard at room temperature. Spectra were processed and least-squares fit using WMOSS4 (40). Quadrupole doublets were fit to Voigt profiles with Lorentzian linewidths of 0.19 mm s^{-1} (full-width at half maximum) and variable Gaussian linewidths. See *SI Appendix*.

ACKNOWLEDGMENTS. We thank P. Roach and T. Stich for useful discussions. We acknowledge the National Institute of General Medical Sciences of the National Institutes of Health for funding (GM111025 to D.L.M.S; GM104543 to R.D.B.; GM65440 to S.P.C.), the Division of Materials Science and Engineering of the Department of Energy (DE-FG02-09ER46632 to J.R.S.) for funding of discussions, protein preparation, and manuscript editing, and the Department of Education (P200A120187 to C.C.P.).

1. Vignais PM, Billoud B (2007) Occurrence, classification, and biological function of hydrogenases: An overview. *Chem Rev* 107(10):4206–4272.
2. Peters JW, Lanzilotta WN, Lemon BJ, Seefeldt LC (1998) X-ray crystal structure of the Fe-only hydrogenase (CpI) from Clostridium pasteurianum to 1.8 angstrom resolution. *Science* 282(5395):1853–1858.
3. Nicolet Y, Piras C, Legrand P, Hatchikian CE, Fontecilla-Camps JC (1999) *Desulfovibrio desulfuricans* iron hydrogenase: The structure shows unusual coordination to an active site Fe binuclear center. *Structure* 7(1):13–23.
4. Lubitz W, Ogata H, Rüdiger O, Reijerse E (2014) Hydrogenases. *Chem Rev* 114(8): 4081–4148.
5. Broderick JB, et al. (2014) H-cluster assembly during maturation of the [FeFe]-hydrogenase. *J Biol Inorg Chem* 19(6):747–757.
6. Vincent KA, Parkin A, Armstrong FA (2007) Investigating and exploiting the electrocatalytic properties of hydrogenases. *Chem Rev* 107(10):4366–4413.
7. Posewitz MC, et al. (2004) Discovery of two novel radical S-adenosylmethionine proteins required for the assembly of an active [Fe] hydrogenase. *J Biol Chem* 279(24): 25711–25720.
8. Mulder DW, et al. (2009) Activation of HydA(ΔEFG) requires a preformed [4Fe-4S] cluster. *Biochemistry* 48(26):6240–6248.
9. Mulder DW, et al. (2010) Stepwise [FeFe]-hydrogenase H-cluster assembly revealed in the structure of HydA(ΔEFG). *Nature* 465(7295):248–251.
10. Kuchenreuther JM, Stapleton JA, Swartz JR (2009) Tyrosine, cysteine, and S-adenosyl methionine stimulate in vitro [FeFe] hydrogenase activation. *PLoS One* 4(10):e7565.
11. Kuchenreuther JM, Britt RD, Swartz JR (2012) New insights into [FeFe] hydrogenase activation and maturase function. *PLoS One* 7(9):e45850.
12. Kuchenreuther JM, George SJ, Grady-Smith CS, Cramer SP, Swartz JR (2011) Cell-free H-cluster synthesis and [FeFe] hydrogenase activation: All five CO and CN^- ligands derive from tyrosine. *PLoS One* 6(5):e20346.
13. Driesener RC, et al. (2010) [FeFe]-hydrogenase cyanide ligands derived from S-adenosylmethionine-dependent cleavage of tyrosine. *Angew Chem Int Ed Engl* 49(9):1687–1690.
14. Shepard EM, et al. (2010) [FeFe]-hydrogenase maturation: HydG-catalyzed synthesis of carbon monoxide. *J Am Chem Soc* 132(27):9247–9249.
15. Betz JN, et al. (2015) [FeFe]-hydrogenase maturation: Insights into the role HydE plays in dithiomethylamine biosynthesis. *Biochemistry* 54(9):1807–1818.
16. Broderick JB, Duffus BR, Duschene KS, Shepard EM (2014) Radical S-adenosylmethionine enzymes. *Chem Rev* 114(8):4229–4317.
17. Kuchenreuther JM, et al. (2014) The HydG enzyme generates an Fe(CO)2(CN) synthon in assembly of the FeFe hydrogenase H-cluster. *Science* 343(6169):424–427.
18. McGlynn SE, et al. (2008) HydF as a scaffold protein in [FeFe] hydrogenase H-cluster biosynthesis. *FEBS Lett* 582(15):2183–2187.
19. Vallese F, et al. (2012) Biochemical analysis of the interactions between the proteins involved in the [FeFe]-hydrogenase maturation process. *J Biol Chem* 287(43): 36544–36555.
20. Czech I, Silakov A, Lubitz W, Happe T (2010) The [FeFe]-hydrogenase maturase HydF from *Clostridium acetobutylicum* contains a CO and CN- ligated iron cofactor. *FEBS Lett* 584(3):638–642.
21. Shepard EM, et al. (2010) Synthesis of the 2Fe subcluster of the [FeFe]-hydrogenase H cluster on the HydF scaffold. *Proc Natl Acad Sci USA* 107(23):10448–10453.
22. Czech I, et al. (2011) The [FeFe]-hydrogenase maturation protein HydF contains a H-cluster like [4Fe4S]-2Fe site. *FEBS Lett* 585(1):225–230.
23. Kuchenreuther JM, et al. (2013) A radical intermediate in tyrosine scission to the CO and CN- ligands of FeFe hydrogenase. *Science* 342(6157):472–475.
24. Driesener RC, et al. (2013) Biochemical and kinetic characterization of radical S-adenosyl-L-methionine enzyme HydG. *Biochemistry* 52(48):8696–8707.
25. Nicolet Y, et al. (2015) Crystal structure of HydG from *Carboxydothermus hydrogenoformans*: A trifunctional [FeFe]-hydrogenase maturase. *ChemBioChem* 16(3): 397–402.
26. Dinis P, et al. (2015) X-ray crystallographic and EPR spectroscopic analysis of HydG, a maturase in [FeFe]-hydrogenase H-cluster assembly. *Proc Natl Acad Sci USA* 112(5): 1362–1367.
27. Nicolet Y, Zeppieri L, Amara P, Fontecilla-Camps JC (2014) Crystal structure of tryptophan lyase (NosL): Evidence for radical formation at the amino group of tryptophan. *Angew Chem Int Ed Engl* 53(44):11840–11844.
28. Pilet E, et al. (2009) The role of the maturase HydG in [FeFe]-hydrogenase active site synthesis and assembly. *FEBS Lett* 583(3):506–511.
29. Nicolet Y, Fontecilla-Camps JC (2012) Structure-function relationships in [FeFe]-hydrogenase active site maturation. *J Biol Chem* 287(17):13532–13540.
30. Xia J, Dong J, Wang S, Scott RA, Lindahl PA (1995) EXAFS, EPR, and electronic absorption spectroscopic study of the alpha-metallo subunit of CO dehydrogenase from *Clostridium thermoaceticum*. *J Am Chem Soc* 117(27):7065–7070.
31. Pandelia M-E, Lanz ND, Booker SJ, Krebs C (2015) Mössbauer spectroscopy of Fe/S proteins. Biochim Biophys Acta - Mol *Cell Res* 1853(6):1395–1405.
32. Kent TA, et al. (1982) Mössbauer studies of beef heart aconitase: Evidence for facile interconversions of iron-sulfur clusters. *Proc Natl Acad Sci USA* 79(4):1096–1100.
33. Krebs C, Broderick WE, Henshaw TF, Broderick JB, Huynh BH (2002) Coordination of adenosylmethionine to a unique iron site of the [4Fe-4S] of pyruvate formate-lyase activating enzyme: A Mössbauer spectroscopic study. *J Am Chem Soc* 124(6):912–913.
34. Telser J, et al. (1995) Cyanide binding to the novel 4Fe ferredoxin from *Pyrococcus furiosus*: Investigation by EPR and ENDOR spectroscopy. *J Am Chem Soc* 117(18): 5133–5140.
35. Zhou C, Holm RH (1997) Comparative isotropic shifts, redox potentials, and ligand binding propensities of [1:3] site-differentiated Cubane-type [Fe4Q4]2+ clusters (Q= S, Se). *Inorg Chem* 36(18):4066–4077.
36. Esselborn J, et al. (2013) Spontaneous activation of [FeFe]-hydrogenases by an inorganic [2Fe] active site mimic. *Nat Chem Biol* 9(10):607–609.
37. Rubach JK, Brazzolotto X, Gaillard J, Fontecave M (2005) Biochemical characterization of the HydE and HydG iron-only hydrogenase maturation enzymes from *Thermatoga maritima*. *FEBS Lett* 579(22):5055–5060.
38. Kuchenreuther JM, et al. (2013) Nuclear resonance vibrational spectroscopy and electron paramagnetic resonance spectroscopy of 57Fe-enriched [FeFe] hydrogenase indicate stepwise assembly of the H-cluster. *Biochemistry* 52(5):818–826.
39. Stoll S, Schweiger A (2006) EasySpin, a comprehensive software package for spectral simulation and analysis in EPR. *J Magn Reson* 178(1):42–55.
40. Prisecaru I (2013) WMOSS4 Mössbauer Spectral Analysis Software (WMOSS), Ver. F. Available at www.wmoss.org. Accessed May 5, 2015.